Parental Conflicting Role Mediates Regulation of The Chromatin Structure in The Mouse Zygote

Masatoshi Ooga (mohga@yamanashi.ac.jp)
University of Yamanashi
Rei Inoue
University of Yamanashi
Sayaka Wakayama
University of Yamanashi
Satoshi Kamimura
University of Yamanashi
Teruhiko Wakayama
University of Yamanashi https://orcid.org/0000-0002-6151-2603

Article

Keywords: zygotes, parental asymmetry, zygotic relaxed chromatin structure, spermiogenesis, spermatozoa, round spermatid, chromatin compaction, chromatin relaxation, intracytoplasmic sperm injection, round spermatid injection

Posted Date: August 26th, 2021

DOI: https://doi.org/10.21203/rs.3.rs-806059/v1

Version of Record: A version of this preprint was published at Communications Biology on July 14th, 2022. See the published version at https://doi.org/10.1038/s42003-022-03623-2.

Parental conflicting role mediates regulation of the chromatin structure in the mouse zygote

Masatoshi Ooga[1, 2, 4], Rei Inoue[2], Sayaka Wakayama[1], Satoshi Kamimura[1, 3] and Teruhiko Wakayama[1]

[1] Advanced Biotechnology Center, University of Yamanashi, Kofu-shi, Yamanashi 400-8510, Japan

[2] Faculty of Life and Environmental Science, University of Yamanashi, Kofu-shi, Yamanashi 400-8510, Japan

[3] Department of Basic Medical Sciences for Radiation Damages, National Institute of Radiological Sciences, National Institutes for Quantum and Radiological Science and Technology, Chiba 263-8555, Japan.

[4] Corresponding author: mohga@yamanashi.ac.jp

Keywords

zygotes, parental asymmetry, zygotic relaxed chromatin structure, spermiogenesis, spermatozoa, round spermatid, chromatin compaction, chromatin relaxation, intracytoplasmic sperm injection, round spermatid injection

Abstract

Parental pronuclei (PN) are asymmetrical in several points but the underlying mechanism for this is still unclear. Recently, a theory has been become broadly accepted that sperm are more than mere vehicles to carry the paternal haploid genome into oocytes. Here, in order to reveal the formation mechanisms for parental asymmetrically relaxed chromatin structure in zygotes, we investigated histone mobility in parthenogenetic-, androgenic-, ROSI-, ELSI-, tICSI-, and ICSI-zygotes with several numbers of PNs with the use of zygotic fluorescence recovery after photobleaching, a method previous established by our group. The results showed that sperm played a role to cause chromatin compaction in both parental PNs. Interestingly, during spermiogenesis, male germ cells acquired this ability and its resistance. On the other hand, oocytes harbored chromatin relaxation ability. Furthermore, the chromatin relaxation factor was competed for between PNs. Thus, these results indicated that the parental asymmetrically relaxed chromatin structure was established as a result of a competition between the PNs for the chromatin relaxation factor that opposed the chromatin compaction effect by sperm. Together, it was suggested that parental germ cells cooperated for their just arisen newborn zygotes by playing a distinct role in the regulation of chromatin structure.

Introduction

During fertilization, parental pronuclei (PN) are formed from the genomes of the sperm and oocyte. Although co-existing in the cytoplasm of the zygote, the PNs are separated before the first mitotic cell cycle and then the two haplotypes fuse to form the new individual genome. There are many differential points in epigenetic factors (e, g histone modifications, histone variants and chromatin relaxation) between PNs before fusion. However, the mechanisms underlying parental asymmetry remain unclear and even less is known about how it is controlled by the interactions between the parental PNs.

The results of our previous study revealed that the chromatin of the male PN derived from the sperm (sp-mPN) was comparatively more relaxed during the preimplantation embryonic stages (Ooga et al., 2016). Interestingly, the chromatin of the female PN (fPN) is significantly less relaxed than that of the sp-mPN. Thus, the relaxation of the zygotic parental chromatin structure is asymmetrical in regard to size (♂ > ♀) (Adenot et al., 1997), transcriptional regulation and activity (♂ > ♀) (Aoki et al., 1997), epigenetic active and repressive of histone markers (♂ < ♀) (Burton et al., 2008) and the amounts of reprogramming factors (♂ > ♀) (Liu et al., 2014). Round spermatid are haploid precursor cells present during the spermatogenetic stage soon after meiosis. Importantly, round spermatid injection (ROSI) and delay of intracytoplasmic sperm injection (ICSI) can result in improper PN formation and subsequent developmental failure during the preimplantation stage (Kishigami et al., 2004b), suggesting that the importance of parental asymmetry. However, the mechanism underlying parental asymmetry has not yet been elucidated. In addition, it is unknown whether relaxation of

63 the asymmetrical parental chromatin is due to an acquisition of greater extent of
64 relaxation of the chromatin of the sp-mPN or compaction of the fPN. Furthermore, the
65 molecules involved in relaxation of the asymmetrical parental chromatin have not yet
66 been identified.

67 It has recently become clear that the spermatozoon also plays a role in the
68 regulation of the embryonic chromatin structure. For example, sperm carry epigenetic
69 factors responsible for the highly complex organization of the genome (Brykczynska et
70 al., 2010; Hammoud et al., 2009; Paradowska et al., 2012) and DNA/histone modification
71 and RNA in the zygote (Yamaguchi et al., 2018; Sharma et al., 2016), which were thought
72 to be involved in the regulation of the establishment of the zygotic chromatin structure
73 and contribute to the control of embryonic development (Trigg et al., 2019; Teperek et
74 al., 2016; Brykczynska et al., 2010; Chen et al., 2021; Sharma et al., 2016). Although the
75 contribution of spermatozoa to the establishment of the zygotic chromatin structure has
76 been widely investigated, it remains unknown not only whether the molecular properties
77 of sperm are involved in establishing the extremely relaxed structure of the sp-mPN
78 chromatin and but also whether these factors are actively involved in establishing the
79 asymmetric relaxation of the parental chromatin after fertilization.

80 Therefore, the aim of the present study was to investigate the mechanisms
81 underlying the asymmetric relaxation of the parental chromatin. The results of this study
82 revealed that sp-mPN harbored the ability to further compact the chromatin of the fPN,
83 resulting in asymmetric relaxation of the parental chromatin structures. In addition to the
84 ability of the sperm to further compact the chromatin, our results indicated that the
85 parental PNs compete to relax the chromatin. Thus, the chromatin structure of the zygote
86 is regulated by the chromatin compaction effect derived from the sperm and the chromatin

87 relaxation effect derived from oocytes in opposition to the sperm-derived compaction
88 effect. Hence, the asymmetrical chromatin relaxation of the zygotic is established by
89 interactions between the parental germ cells.
90
91
92

Results

Sperm causes compaction of both parental chromatin structures

We previously reported that asymmetric relaxation of the parental chromatin was established in the late zygotic stage of the embryo at 10–12 hours post insemination (hpi) (Ooga et al., 2016). First, we confirmed the reproducibility of asymmetric relaxation of the parental chromatin (♂ > ♀) in zygotes obtained by in vitro fertilization (IVF) (**Fig. S1**) and ICSI. In addition, the mechanisms causing the parental asymmetric pattern were investigated by determining whether sp-mPN acquired the highly relaxed or fPN obtained the compacted chromatin structure. To this end, the dynamics of chromatin relaxation during the early to mid-zygotic stages were examined with the use of parthenogenetically activated- and ICSI-derived zygotes. Although the chromatin of the fPN was gradually compacted along with the development of the zygote, there was no significant change in the chromatin of the sp-mPN (**Fig. 1A and B**). Importantly, in the presence of sperm/sp-mPN, the chromatin of the fPN was further compacted. As a result, the parental asymmetric pattern (♂ > ♀) was established by 8 hpi. The dependency of fPN compaction on sp-mPN was confirmed by enucleation of the sp-mPN followed by immuno-staining of histone 3 lysine 9 trimethylation (H3K9me3) as a marker of the fPN (**Fig. 1C and S2**). Collectively, these findings suggest that the asymmetrical structure of the parental chromatin was established via acquisition of the compacted chromatin structure of the fPN by a mechanism dependent on the sperm/sp-mPN.

Next, in order to determine whether the mechanisms underlying sp-mPN-dependent chromatin compaction were also activated in the sp-mPN itself, 1PN-ICSI were constructed by ICSI with enucleated MII oocytes (**Fig. 1D**). The chromatin of a

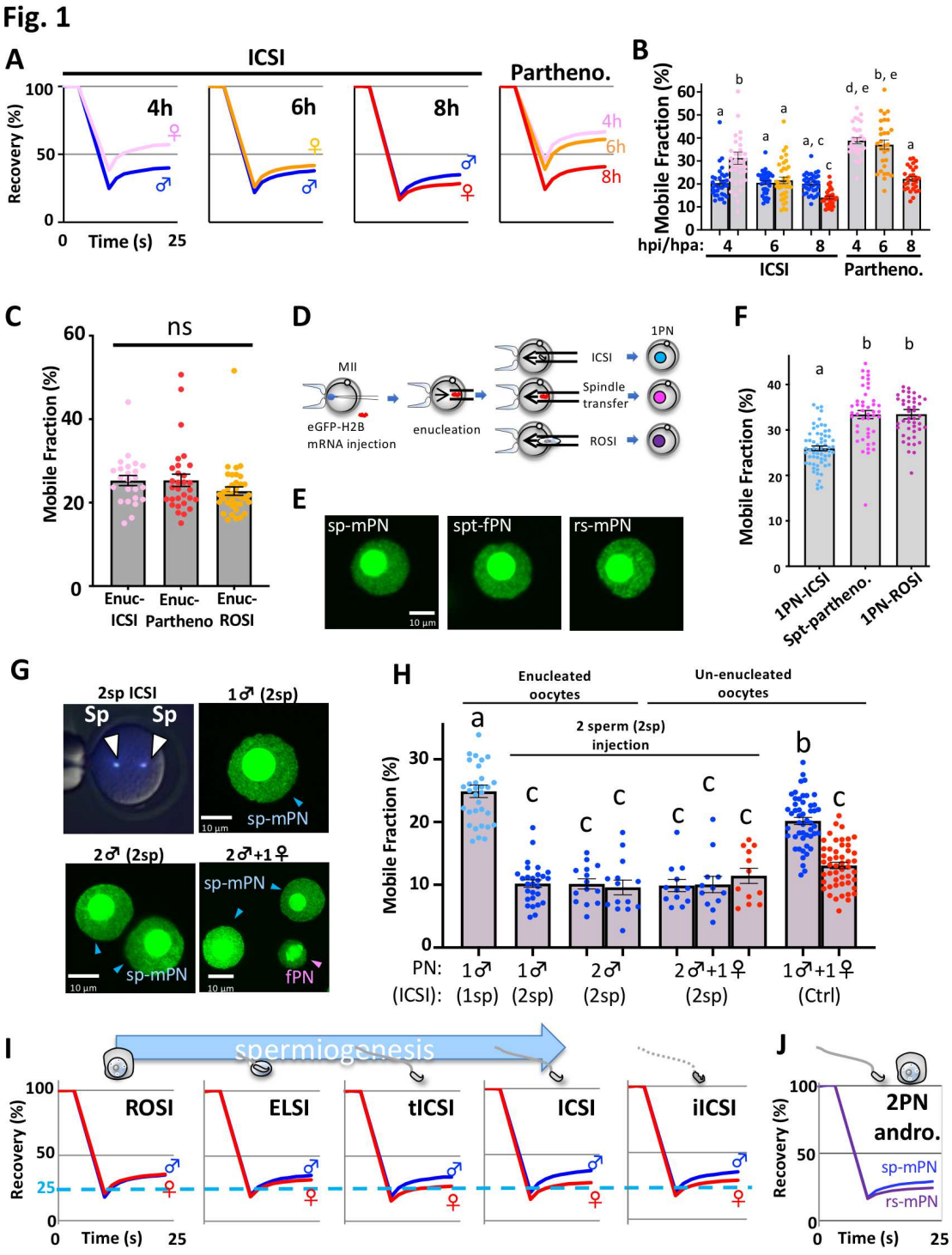

Fig. 1. ***Sperm causes compaction of both parental chromatin structures***

(**A** and **B**) Dynamics of chromatin relaxation during the early and mid-stages of ICSI and parthenogenetically activated zygotes. zFRAP analysis was performed at 4, 6, and 8 hpi or hpa. A recovery curve indicating the average fluorescence recovery rate is shown

(A). The average mobile fraction (MF) is shown as a gray bar (B). Single dots indicate the MF score of each male and female pronuclei (mPN, fPN), respectively. Blue, mPN; pink, fPN-4h; orange, fPN-6h; and red, fPN-8h. For parthenogenetic (partheno)-zygotes with 2PN, the average MF score is shown. Error bar indicates the standard error (SE). (**C**) mPN was enucleated at 4 hpi/hpa from ICSI- and ROSI-zygotes. Two PN partheno-zygotes were prepared as controls. The remaining fPN was subjected to zFRAP analysis at 8 hpi/hpa. (**D**) Illustration of the preparation of 1PN-zygotes (**E**) Fluorescence images of each single PN: sperm-derived mPN (sp-mPN), spindle transfer-derived fPN (spt-fPN), and round spermatid-derived mPN (rs-mPN) (**F**) Average MF scores of 1PN-ICSI, -ROSI, and spt-partheno. (**G**) Two sperm were injected into enucleated MII oocytes (upper-left). Sperm (sp) were stained with Hoechst 33342. Fluorescence images of PNs: "1♂ (2sp)" and "2♂ (2sp)" indicate the one and two male PN-zygotes injected with two sperm (2sp), respectively (upper right and lower left). Two sperm injected into un-enucleated MII oocytes (2♂ + 1♀; lower right). (**H**) Average MF scores of the zygotes as shown in (**G**). As a control, one sperm was injected into enucleated MII- (same as 1PN-ICSI in Fig. 1 F; "1♂(1sp)")) and normal ICSI-zygotes (1♂ + 1♀). Blue and red dots indicated mPN and fPN, respectively. (**I**) Recovery curve of ROSI-, ELSI-, tICSI-, ICSI-, and iICSI-zygotes. (**J**) Recovery curve of androgenic zygotes prepared by co-injetion of sperm and round spermatid.

single sp-mPN was more compact than a single fPN of parthenogenetic zygotes, although both appeared similar, suggesting that the chromatin compaction mechanism of sp-mPN worked on its own (**Fig. 1E, F and S3**). Further confirmation by ICSI was conducted with the use of enucleated MII oocytes fertilized with two sperm (2sp) (i.e., **"1♂ (2sp)**"and "**2♂ (2sp)**" in **Fig. 1G, H and S4)**, which showed that the additional sperm resulted in further chromatin compaction in each sp-mPN, as the chromatin of zygotes formed by ICSI with two sperm and an enucleated MII oocyte was more compact than that of the zygotes formed by one sperm ("**1♂ (1sp)**," light blue in **Fig. 1F and H**). In zygotes formed by ICSI with two sp-mPNs and an "un-enucleated" oocyte ("**2♂ + 1♀**"), two sp-mPNs were comparable to one fPN and disruption of the parental asymmetric pattern (♂≒♀). Importantly, there was no significant difference between the fPNs of 2♂+1♀ and that of 1♂+1♀ (ctrl), indicating that the chromatin of the fPNs was already compacted to almost the possible limit even in the presence of only one sperm. On the other hand, to compact the chromatin of sp-mPN to this level, at least two sperm were needed. Thus, the sp-mPN exhibited innate resistance to chromatin compaction. Together, these results suggest that although the chromatin compaction effect works on the chromatin of both parental PNs, asymmetric relaxation of the parental chromatin was established due to differences in sensitivity to this effect. The zygotes harboring two fPNs with a single sp-mPN ("**1♂ + 2♀**") still exhibited the parental asymmetric pattern (**Fig. S5**). Thus, the additional chromatin from the fPN failed to disrupt the parental asymmetric pattern.

To examine where the ability for the chromatin compaction in both parental PNs was acquired among the stages during spermiogenesis, zygotic

fluorescence recovery after photobleaching (zFRAP) analysis of zygotes fertilized by various micro-insemination methods (ROSI, ELSI, tICSI, and ICSI) was performed at 8 hpi or hours post micro-activation (hpa). All male PNs of zygotes obtained by ROSI and ICSI exhibited similar levels of chromatin relaxation (**Fig. 1I and Fig. S6A)**. By contrast, the extent of chromatin relaxation of the fPNs of these zygotes was decreased along with the maturity of the male germ cells. Thus, the maturity of spermatogenic cells is correlated with the asymmetric structure of the parental chromatin. The asymmetric structure of the parental chromatin in zygotes obtained by ICSI with the use of inactivated sperm (iICSI-zygotes) was only slightly decreased as compared to that of the ICSI-zygotes (**Fig. 1I and Fig. S6B)**, indicating that asymmetric relaxation of the parental chromatin acquired during spermiogenesis could not be explained by the activation capacity of the oocyte. Taken together, these results suggest that sperm has the ability to compact the chromatin of both parental PNs and resistance to compaction leads to parental asymmetrically relaxed chromatin structure during spermiogenesis. Correct discrimination of parental chromatin in ROSI-zygotes was confirmed by zFRAP analysis with paternal PNs from enucleated zygotes followed by immunocytochemical analysis of H3K9me3 as a marker of the fPNs (**Fig. S7**). The inability of round spermatid to compact chromatin was confirmed by 1PN-ROSI, which showed a comparable level of chromatin relaxation of 1PN-parthenogenetic zygotes (**Fig. 1F**, purple). In addition, 2PN androgenic zygotes formed by sp-mPN, with comparatively greater chromatin relaxation, and round spermatid-derived from the male PN (rs-mPN), with relatively less chromatin relaxation (**Fig. 1J and S8**), indicated that the round spermatid had not yet acquired resistance to chromatin compaction. Furthermore, in the presence of sp-mPN, the chromatin of the rs-mPN was condensed to the same level as that of the fPN (**Fig. S9**). These findings were

187 consistent with the disruption of the asymmetric structure of the parental chromatin in
188 zygotes obtained by ROSI.
189
190 ***Parental PNs compete for chromatin relaxation factors***
191 As shown in **Fig. 1F** and **H**, the chromatin of 1PN-zygotes and even 1PN ICSI-
192 zygotes, was extremely relaxed as compared to that of ICSI-zygotes with two parental
193 PNs (1♂ (1sp) vs. 1♂ + 1♀ (1sp)). The results of our previous study revealed that
194 oocytes harbored highly loosened chromatin structures and chromodomain helicase DNA
195 binding protein 9 (CHD9), which regulates chromatin remodeling, participated in the
196 regulation of the chromatin relaxation (Ooga et al., 2018b). Furthermore, in another
197 previous study, the transferred somatic cell nuclei into enucleated oocytes acquired a
198 relaxed chromatin structure, indicating the presence of factors promoting chromatin
199 relaxation in oocytes and zygotes (Ooga et al., 2016). These findings prompted the
200 hypothesis that the concentration of factors promoting chromatin relaxation into a single
201 PN led to the extremely relaxed chromatin structure. At the same time, such factors were
202 distributed to the parental PNs. To examine this possibility, parthenogenetically activated
203 oocytes were constructed with various numbers of fPNs (1, 2, and 4 fPNs; **Fig. 2A**), which
204 enabled exclusion of the sp-mPN-derived chromatin compaction effect. As expected, the
205 extent of chromatin relaxation decreased along with the increase in the number of PNs
206 and the fPNs in the same zygotes showed similar level of chromatin relaxation (**Fig. 2B**
207 **and S10**). These results suggest that the chromatin relaxation factors are present in the
208 zygotes and at least, in parthenogenetic zygotes, the fPNs competed for these factors.
209 If the parental PNs compete for factors that promote chromatin relaxation, the
210 lack of one parental PN should cause excess chromatin relaxation in another. Therefore,

Fig. 2

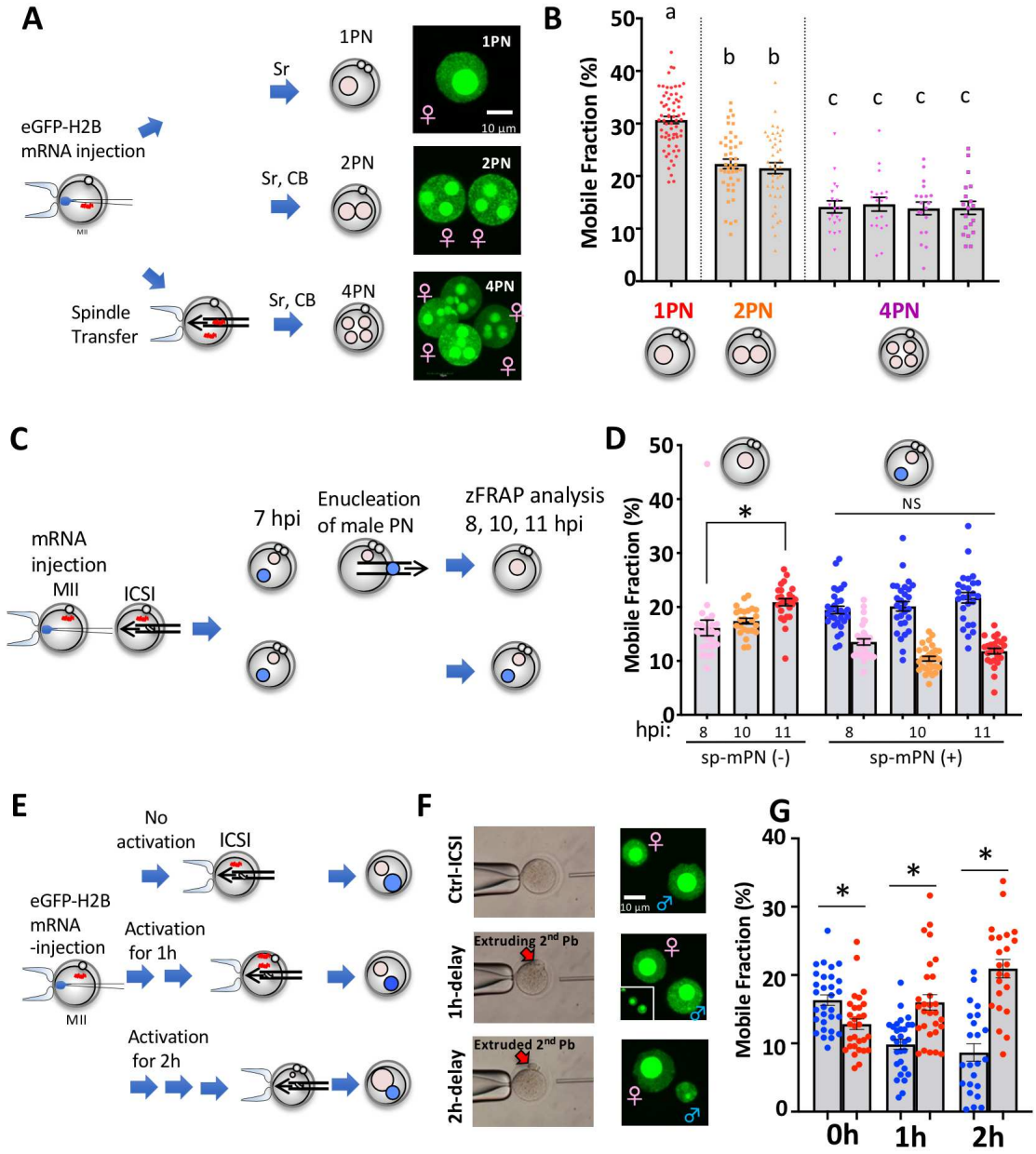

Fig. 2. ***Parental PNs compete for chromatin relaxation factors***

(**A**) Illustration of the preparation of 1, 2, and 4PN partheno-zygotes and fluorescence images of the fPNs (**B**) Average MF scores of the partheno-zygotes prepared as shown in (**A**). (**C**) Illustration of the preparation of sp-mPN-enucleated partheno-zygotes. (**D**) Average MF scores of the zygotes prepared as shown in (**C**). Blue, mPN; pink, fPN-8h; orange, fPN-10h; and red, fPN-11h). Asterisks indicate significant differences. (**E**)

Illustration of the preparation of delay ICSI-zygotes. “Sr” indicates strontium. (**F**) Control and delay ICSI are shown. The second polar body is indicated with a red arrow. Fluorescence images of the mPN and fPN. The inset shows lower magnification images of the second polar body near the fPN. (**G**) Average MF scores of the delay ICSI-zygotes prepared as shown in (**E**, **F**).

the potential of excess chromatin relaxation in fPN was investigated with the use of enucleation of sp-mPNs. In sp-mPN-enucleated-zygotes, chromatin relaxation of the fPN gradually increased along with the progression of zygotic development (**Fig. 2C and D**). In contrast, zFRAP analysis of ICSI-zygotes at 8, 10, and 11 hpi showed that the extent of chromatin relaxation was maintained in both parental PNs. Thus, the parental PNs competed for the chromatin relaxing factors. Next, the effect of delayed PN formation (Kishigami et al., 2004b) on parental asymmetry was investigated. To this end, delayed-ICSI zygotes were constructed and then analyzed by zFRAP (**Fig. 2E**). Observation of PN formation of delayed-ICSI zygotes revealed the reversal of PN size, larger or smaller, between parental PNs (**Fig. 2F**). zFRAP analysis revealed that asymmetric relaxation of the parental chromatin was compromised along with an increased delay time of ICSI (**Fig. 2G and S11**). Particularly, almost all of the 2 h-delayed-ICSI zygotes showed a reversed parental asymmetric pattern (♂ < ♀). A delay of only 1 h resulted in a considerable change in PN size and the chromatin of the fPN was more relaxed than that of the sp-mPN. Collectively, these results indicate that parental PNs compete for chromatin relaxing factors and the state of the zygotic chromatin is regulated by an antagonistic balance between the chromatin compaction effects derived from the sperm and the relaxation effect from the oocyte. Furthermore, it is possible that the sp-mPN might have obtained more such relaxation factors than the fPN, resulting in self resistance to the chromatin compaction effect.

More chromatin relaxer was utilized in sp-mPN than fPN.

Finally, three types of RNA polymerase inhibitors (i.e., actinomycin D (“Act D”; Pol I inhibitor), alpha-amanitin (“Ama”; Pol II inhibitor), and Pol III inhibitor (Pol

248 IIIi) were employed to determine whether chromatin relaxation factors are produced by
249 zygotic transcription. Ama slightly, but not significantly, increased the extent of
250 chromatin relaxation (**Fig. S12)**, indicating that the chromatin relaxation factors were not
251 derived from Pol II-transcribed mRNA. However, both Act D (**Fig. 3A and B)** and Pol
252 lIli (**Fig. 3C and D)** caused significant compaction of the chromatin in the only sp-mPN.
253 Thus, relaxation of the chromatin of the sp-mPN was more sensitive to these inhibitors
254 than that of the fPN, suggesting that more chromatin relaxation factors were utilized the
255 in sp-mPN. Furthermore, since Pol I and III produce RNA that is involved in translation,
256 it is possible that chromatin relaxation factors are proteins, such as H1foo (Funaya et al.,
257 2018), presumably also supplied by zygotic translation of maternally stored mRNA.
258
259

Fig. 3

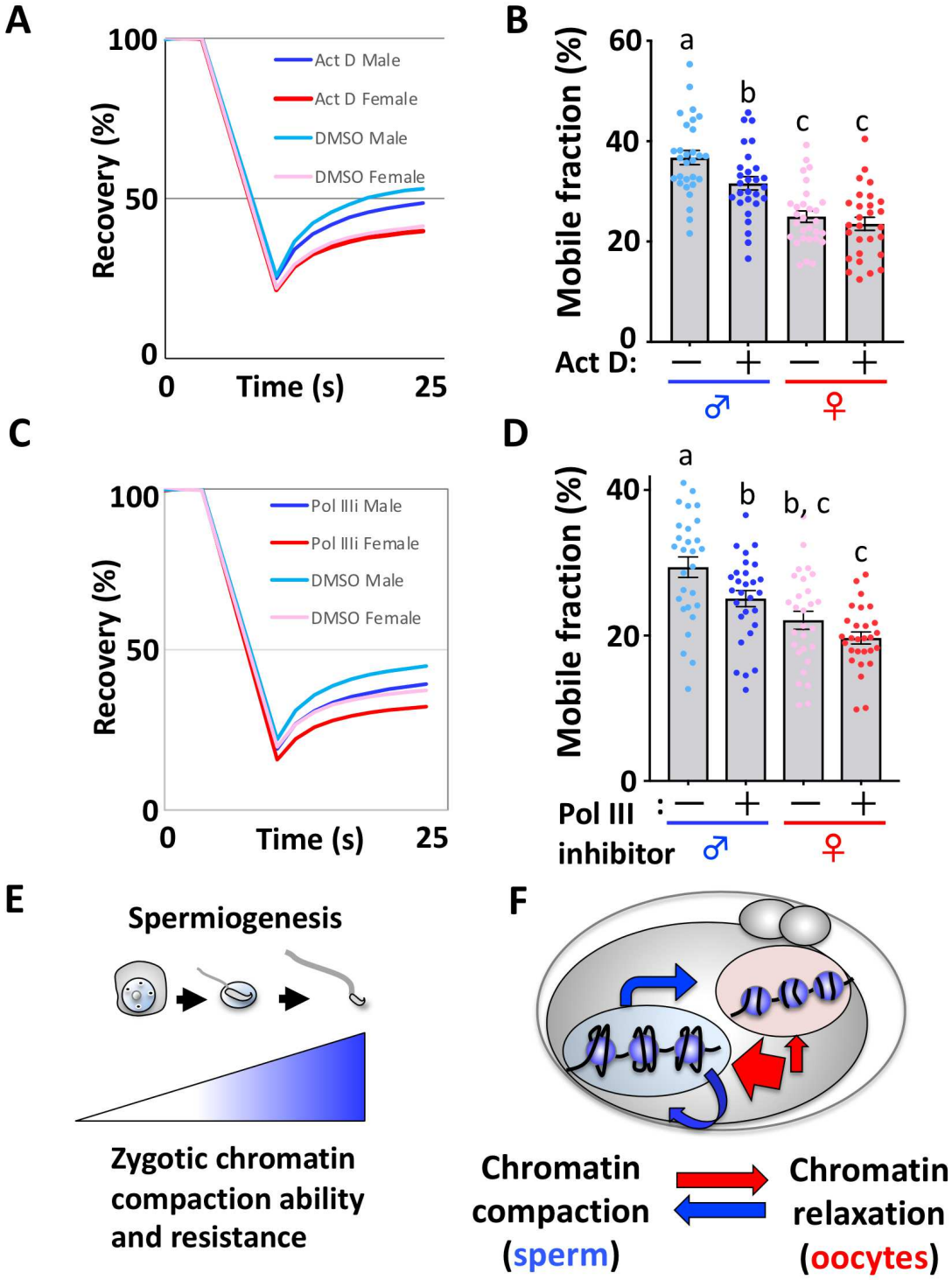

Fig. 3. *More chromatin relaxer was utilized in sp-mPN than fPN*

(**A**) Recovery curve of IVF zygotes treated with 0.1 μg/ml Act D. Control zygotes were treated with 1% dimethyl sulfoxide (DMSO). (**B**) Average MF scores of IVF zygotes treated with Act D and DMSO. (**C**) Recovery curve of IVF-zygotes treated with 20 μM Pol IIIi. Control zygotes were treated with 0.1% DMSO. (**D**) Average MF scores of IVF zygotes treated with Pol IIIi and 0.1% DMSO. (**E**) Schematic illustration indicating that male germ cells acquire the ability to compact chromatin and resistance during spermiogenesis. (**F**) In the zygotes, the sperm-derived chromatin compaction effect and oocyte-derived chromatin relaxation factors are antagonistic. Probably, more chromatin relaxation factors caused a more relaxed state and conferred resistance to chromatin compaction in the sp-mPN.

Discussion

In this study, the mechanisms underlying asymmetric relaxation of the parental chromatin were investigated, which revealed that sperm have the ability to compact the chromatin of both parental PNs (**Fig. 1A–H**). Interestingly, the abilities to promote and resist chromatin compaction are acquired during spermiogenesis (**Fig. 1I, J and 3E**). In addition to the ability to compact chromatin, zygotes also harbor factors that promote chromatin relaxation, which the parental PNs compete for (**Fig. 2A–G**) and are presumably dependent on zygotic translation of maternally pooled mRNA (**Fig. 3A–D**). Thus, asymmetrically relaxed chromatin of the zygote is established via the mature male and female germ cells (**Fig. 3F**), and is possibly determined by a balance between them. Hereafter, this power balance is referred to as "parental epigenetic competition."

In 1PN-ICSI zygotes, the sp-mPN demonstrated less chromatin relaxation than that of the 1PN-ROSI and spindle-transferred haploid-parthenogenetically activated oocytes (**Fig. 1F and S3**). This result indicated that sperm actively condense the chromatin structure. In **Fig. 1I and S6**, although NaOH-treated inactivated sperm lost the ability to activate the oocyte, the ability to compact the chromatin was retained, indicating that the unidentified sperm-derived chromatin condensing factors are not associated with the sperm surface. A recent broadly accepted theory states that sperm are more than mere vehicles to carry the paternal haploid genome into the oocyte. Indeed, sperm carried huge kinds of RNA into oocytes at fertilization. several studies showed during epididymal transit from testis to cauda epididymis, sperm obtained small RNA payload (Sharma 2019; Trigg et al., 2019). Since tICSI-zygotes, which have no such RNA payload, exhibit asymmetric relaxation of the parental chromatin, the RNA payload of the mature sperm might not be involved in compaction of the zygotic chromatin. However, the possibility

297 that sperm RNA is involved in compaction of the chromatin compaction must still be
298 considered. Reportedly, sperm RNA is deeply embedded in the sperm head (Yan et al.,
299 2008). Such RNA is not easy to extract and NaOH treatment did not completely dissolve
300 the sperm head, indicating that the RNA was not eliminated (Schuster et al., 2016). In
301 addition to the embedded RNA, proteins are possibly the responsible factors. Following
302 the initiation of spermiogenesis, during which there is no transcription, specific stored
303 RNAs were translated to proteins (Rathke et al., 2014). Since our results indicated that
304 the ability of sperm to compact chromatin is acquired after the initiation of
305 spermiogenesis, it is also possible that newly synthesized proteins at this phase are
306 responsible for chromatin compaction. To understand the importance and mechanisms of
307 parental epigenetic competition, further studies are needed to test this hypothesis and to
308 identify the RNA and/or protein molecules responsible for zygotic chromatin compaction.
309 It is possible that there are differences in the dynamics of PN formation
310 involved in the regulation of parental epigenetic competition. The establishment of the
311 chromatin structure of the sp-mPN is very distinct from that of the fPN. Within 1 h after
312 fertilization, maternally pooled histone proteins are rapidly incorporated into the sp-mPN,
313 resulting in the sperm head becoming decondensed and expanded [21]. On the other hand,
314 at this phase, maternal genetic materials still form completely condensed meiotic
315 chromosomes, which are located in the cytoplasm or the going to be extruded second
316 polar body (**Fig. 2F**; Ooga et al., 2008). Also, it is widely thought that the transcription
317 factors and chromatin remodeling factors dissociate from the condensed chromosomes
318 and are re-recruited to the re-organized chromatin structure after chromosome
319 segregation [23]. Therefore, it is likely that maternal factors were first taken up by the sp-
320 mPN and then later by the fPN. In 1 h-delayed-ICSI-zygotes, the asymmetric relaxation

of the parental chromatin structure was reversed (**Fig. 2G and S11**). This experiment was designed to collapse the competition for the maternally supplied factors from the ooplasm and resulted in reversal of the parental asymmetry. Thus, it is possible that more maternally pooled or newly produced zygotic factors were incorporated into the sp-mPN than the fPN in normally fertilized zygotes. Indeed, more reprogramming factors that confer totipotency to the somatic cell nuclei are reportedly incorporated into the sp-mPN than the fPN (Liu et al., 2014). Accordingly, it is plausible that more maternally supplied chromatin relaxation factors could be incorporated into the sp-mPN than the fPN, resulting in asymmetric relaxation of the parental chromatin.

Round spermatids do not harbor the ability to compact the chromatin (**Fig. 1F and S3**). Moreover, when compared, in 1PN-zygotes, rs-mPNs and fPNs, which are derived from transferred meiotic spindles, exhibited the same level of chromatin relaxation. However, there was significant asymmetric relaxation of the parental chromatin in ROSI-zygotes (**Fig. 1I, S6**). Our ROSI-zygote production strategy employed a "post-activation protocol" (Kishigami et al., 2004a) to improve the rate of 2PN formation (Kishigami et al., 2004b). In this protocol, the oocytes injected with round spermatids were activated within 30 min after ROSI. As a result, the round spermatid genome was able to avoid premature chromatin condensation followed by extrusion of the pseudo polar body. Thus, chromosome condensation and incorporation of maternal factor did not seem to be equal between the rs-mPN and fPN, suggesting the possibility that the rs-mPN harbored more chromatin relaxation factors than the fPN (**Fig. S13**). Collectively, these findings suggest that it is probable that the differences in dynamics during PN formation contribute to the parental epigenetic competition.

344 The results of this study indicated that the sperm or sp-mPN exerted chromatin
345 compaction effects in both parental PNs. This finding raises the question of the biological
346 significance of zygotic chromatin compaction by sperm. Bui et al. reported that sperm
347 have the ability to regulate transcriptional activity (Bui et al., 2011). Thus, sperm play an
348 important role in the regulation of zygotic genome activation (ZGA). Chromatin
349 compaction by sperm might be involved in regulation of ZGA. It was thought that
350 promiscuous transcription occurs during minor ZGA and correlates with extensive
351 chromatin relaxation by FRAP (Abe et al., 2018). Our results demonstrated that sperm-
352 derived chromatin compaction factors condense the paternal chromatin structure in the
353 sp-mPN and then the extent of chromatin relaxation becomes comparable to that of the
354 rs-mPN, indicating that in the absence of sperm-derived chromatin condensing factors,
355 the paternal chromatin structure derived from the sperm should be extremely relaxed.
356 Then, it is possible that such an extreme chromatin structure will cause abnormalities to
357 the transcriptome during ZGA. To assess this possibility, the chromatin compaction
358 factors must be identified with the use of a knockdown/knockout experimental system,
359 which was not possible in the current study.
360 We also observed abnormal chromatin relaxation in the ROSI-zygotes.
361 Therefore, it would be beneficial to analyze the transcriptome of ROSI-derived embryos
362 to understand biological role of chromatin relaxation. The results of this study confirmed
363 that that sperm actively participate in the regulation of asymmetric relaxation of the
364 parental chromatin structure. However, the reason why the chromatin of the mPN is more
365 relaxed than that of the fPN remains unclear. Hence, comparative analysis with RNA-seq
366 of control- and 1 h-delay-ICSI-zygotes is warranted. Nonetheless, further investigations
367 are needed to understand the significance of parental epigenetic competition.

Materials and methods

Animals

Eight to 12-week-old female B6D2F1 (C57BL/6 × DBA2) (n = 102) and 10–14-week-old male ICR (n = 42) mice (SLC, Shizuoka, Japan) were used as oocyte and spermatozoa donors, respectively. All animal experiments were approved by the Ethics Committee of the University of Yamanashi (reference number: A29-24) and conducted in accordance with Guide for the Care and Use of Laboratory Animals and the ARRIVE guidelines. All mice were housed under specific pathogen-free conditions at a constant temperature of 25°C, relative humidity of 50%, and a 14/10-h light/dark period with ad libitum access to a commercial diet and distilled water. In this study, body weight was not measured because the body weight of young mice has no effect on embryo quality.

ICSI and ROSI

Obtained cumulus cells and oocyte complexes were treated with hyaluronidase for 10 min and the denuded oocytes were collected. For ICSI, spermatozoa were obtained from the cauda epididymis and then cultured in human tubal fluid [27] for capacitation. Prior to cytosolic injection of the denuded oocytes, the sperm tails were eliminated with a Piezo drive micromanipulator (Prime Tech Ltd., Ibaraki, Japan) in CZB-HEPES medium supplemented with 10% PVP (10% PVP-CZB-HEPES) (Chatot et al., 1990). The zona pellucida and cytosolic membranes were also disrupted with a Piezo drive micromanipulator. For ROSI, ELSI, and testicular ICSI, the harvested testes were minced with scissors, sieved through a Mini Cell Strainer, and then re-suspended in 10% PVP-CZB-HEPES. The nucleus of each round spermatid was collected with a narrow pipette

with a diameter of 7–8 μm. The zona pellucida and cytosolic membrane were disrupted in the same manner as for ICSI. The oocytes injected with round spermatid were activated by culturing in Ca^{2+}-free CZB medium containing 5 mM $SrCl_2$ for 1–2 h. The tails of the testicular sperm were also cut with a Piezo drive micromanipulator as with ICSI.

Enucleation and injection of the nuclei of oocytes

Freshly collected oocytes were transferred into 5 μg/μl of cytochalasin B (CB) containing HEPES-buffered CZB. After 10 min, the nuclei were aspirated with a glass capillary tube (Wakayama et al., 2019). After enucleation, the ooplasm was washed and cultured in CZB until micro-insemination. In some experiments, the aspirated nuclei were injected into enucleated ooplasms or un-enucleated MII oocytes in CB containing HEPES-buffered CZB (Konno et al., 2020).

Enucleation of male PN

Before enucleation, the zygotes with two PNs at 7 hpi were cultured in KSOM (Lawitts et al., 1993) containing CB for 20 min. The zygotes were then transferred into CB containing HEPES-buffered CZB. The larger PN and furthest away from the second polar body was deemed the mPN, which was aspirated from the zygote. The enucleated zygotes were washed and cultured in KSOM.

Delay ICSI

Collected oocytes were subjected to parthenogenetic activation in Ca^{2+}-free CZB medium containing 5 mM $SrCl_2$. After 1 h, the activated oocytes with extruding second polar bodies were collected for micro-insemination with capacitated spermatozoa.

At 2 h after activation, the zygotes with an obvious extruded second polar body were used for micro-insemination.

In vitro fertilization

Spermatozoa were obtained from ICR mice. For capacitation, the spermatozoa were cultured for 1 h before insemination. Cumulus cells and oocyte complexes were obtained from super-ovulated BDF1 female mice by injection of 7.5 IU of equine chorionic gonadotropin (ASKA Pharmaceutical Co., Ltd., Tokyo, Japan) and human chorionic gonadotropin (ASKA Pharmaceutical) at 46–50-h intervals. Cumulus cells and oocyte complexes were inseminated with capacitated sperm in human tubal fluid medium supplemented with bovine serum albumin (BSA; Sigma-Aldrich Corporation, St. Louis, MO, USA) at 3 mg/ml. At 1-2 h post-insemination, the zygotes were washed and cultured in KSOM medium under humidified atmosphere of 5% CO_2/95% air at 38ºC.

Synthesis of mRNA

The plasmid "pTOPO eGFP-H2B" (Ooga et al., 2016) encoding enhanced green fluorescent protein (eGFP)-fused histone H2B was linearized by *Not*1 overnight. Afterward, the plasmid was purified with phenol/chloroform and then precipitated with ethanol. Purified DNA was dissolved in nuclease-free water as template DNA for subsequent in vitro transcription with using mMESSAGE MACHINE sp6 kit (Themo Fisher Scientific, MA, USA). Synthesized mRNA was then processed with a poly A tailing kit (Themo Fisher Scientific). The mRNA with a poly A tail was purified and precipitated with lithium chloride precipitation solution, dissolved, and stored at 500 ng/μl and −80ºC until use.

Zygotic fluorescence recovery after photobleaching (zFRAP) analysis

mRNA encoding eGFP-H2B (250 ng/μl) was prepared as shown above and injected into the cytoplasm of unfertilized MII oocytes or zygotes at 1–2 h after insemination. mRNA-injected MII oocytes were then micro-inseminated with a round spermatid, elongated spermatid, or spermatozoa. At 8 h post-insemination or -activation, the zygotes were collected for zFRAP analysis, which was performed as described previously (Ooga and Wakayama 2017; Ooga et al., 2018a), and observed under a confocal microscope (FV1200; Olympus Corporation, Tokyo, Japan). The mobile fraction was assessed as described in our previous study.

Immuno-staining

After zFRAP analysis and observation, the zygotes were fixed with 4% paraformaldehyde containing 0.2% Triton X-100 for 20 min. After washing three times with PBS containing 1% BSA and 0.2% Tween 20, the zygotes were incubated with primary antibodies against H3K9me3 (ab8898; Abcam, Cambridge, MA, USA) diluted in PBS containing 1% BSA and 0.1% Triton X-100 at 4˚C overnight. After washing three times with PBS containing 1% BSA and 0.2% Tween 20, the zygotes were incubated with a secondary antibody (Alexa 568 conjugated anti rabbit IgG mouse IgG). The stained zygotes were mounted on PBS containing 4',6-diamidino-2-phenylindole.

Statistical analysis

All statistical analyses were performed using Prism 9 software (GraphPad Software, Inc., San Diego, CA, USA) with one-way analysis of variance (ANOVA)

followed by Tukey's multiple comparisons test or the paired *t*-test (for parental asymmetry analysis). A probability (*p*) value of <0.05 was considered statistically significant.

Competing interest statement

The authors have no competing interests to declare.

Acknowledgments

We thank Drs. S. Funaya, Y. Fujimoto, Mr. K. Kazama, D. Ito, Y. Kikuchi, M. Nakamura, and Miss C. Yamaguchi for critical and useful comments on the manuscript. Financial support for this research was provided by a Grant-in-Aid for Young Scientists (grant no. 19K16012) and Research Grant for Young Scholars funded by Yamanashi Prefecture to M.O., the Asada Science Foundation and the Canon Foundation (grant no. M20-0006) to T.W.

Author contributions.

M.O and T.W conceived and designed this study. M.O. performed most of the experiments and R.I., S.W. and S.K. performed some of the experiments. M.O., R.I., S.W., S.K., and T.W. analyzed all data. M.O. and T.W. wrote the manuscript. All authors read and edited the manuscript.

References

1. Ooga, M., Fulka, H., Hashimoto, S., Suzuki, M. G. & Aoki, F. Analysis of chromatin structure in mouse preimplantation embryos by fluorescent recovery after photobleaching. *Epigenetics* **11**, (2016).

2. Adenot, P. G., Mercier, Y., Renard, J. P. & Thompson, E. M. Differential H4 acetylation of paternal and maternal chromatin precedes DNA replication and differential transcriptional activity in pronuclei of 1-cell mouse embryos. *Development* **124**, 4615–4625 (1997).

3. Aoki, F., Worrad, D. M. & Schultz, R. M. Regulation of transcriptional activity during the first and second cell cycles in the preimplantation mouse embryo. *Dev. Biol.* **181**, 296–307 (1997).

4. Burton, A. & Torres-Padilla, M. E. Epigenetic reprogramming and development: A unique heterochromatin organization in the preimplantation mouse embryo. *Brief. Funct. Genomics* **9**, 444–454 (2010).

5. Liu, W. *et al.* Asymmetric Reprogramming Capacity of Parental Pronuclei in Mouse Zygotes. *Cell Rep.* **6**, 1008–1016 (2014).

6. Kishigami, S., Wakayama, S., Nguyen, V. T. & Wakayama, T. Similar time restriction for intracytoplasmic sperm injection and round spermatid injection into activated oocytes for efficient offspring production. *Biol. Reprod.* **70**, 1863–9 (2004).

7. Brykczynska, U. *et al.* Repressive and active histone methylation mark distinct promoters in human and mouse spermatozoa. *Nat. Struct. Mol. Biol.* **17**, 679–687 (2010).

8. Hammoud, S. S. *et al.* Distinctive chromatin in human sperm packages genes for embryo development. *Nature* **460**, 473–478 (2009).

9. Paradowska, A. S. *et al.* Genome wide identification of promoter binding sites for H4K12ac in human sperm and its relevance for early embryonic development. *Epigenetics* **7**, 1057–1070 (2012).

10. Yamaguchi, K. *et al.* Re-evaluating the Localization of Sperm-Retained Histones Revealed the Modification-Dependent Accumulation in Specific Genome Regions. *Cell Rep.* **23**, 3920–3932 (2018).

11. Sharma, U. *et al.* Biogenesis and function of tRNA fragments during sperm maturation and fertilization in mammals. *Science (80-.).* **351**, 391–396 (2016).

12. Trigg, N. A., Eamens, A. L. & Nixon, B. The contribution of epididymosomes to the sperm small RNA profile. *Reproduction* vol. 157 R209–R223 (2019).

13. Teperek, M. *et al.* Sperm is epigenetically programmed to regulate gene

transcription in embryos. *Genome Res.* **26**, 1034–1046 (2016).

14. Chen, X. *et al.* Human sperm tsRNA as potential biomarker and therapy target for male fertility. *Reproduction* **161**, 111–122 (2021).

15. Ooga, M. *et al.* Chd9 mediates highly loosened chromatin structure in growing mouse oocytes. *Biochem. Biophys. Res. Commun.* **500**, 583–588 (2018).

16. Funaya, S., Ooga, M., Suzuki, M. G. & Aoki, F. Linker histone H1FOO regulates the chromatin structure in mouse zygotes. *FEBS Lett.* **592**, (2018).

17. Sharma, U. Paternal contributions to offspring health: Role of sperm small rnas in intergenerational transmission of epigenetic information. *Front. Cell Dev. Biol.* **7**, 1–15 (2019).

18. Yan, W. *et al.* Birth of mice after intracytoplasmic injection of single purified sperm nuclei and detection of messenger RNAs and microRNAs in the sperm nuclei. *Biol. Reprod.* **78**, 896–902 (2008).

19. Schuster, A. *et al.* SpermBase: A Database for Sperm-Borne RNA Contents. *Biol. Reprod.* **95**, 99–99 (2016).

20. Rathke, C., Baarends, W. M., Awe, S. & Renkawitz-Pohl, R. Chromatin

538 dynamics during spermiogenesis. *Biochim. Biophys. Acta - Gene Regul. Mech.*
539 **1839**, 155–168 (2014).
540 21. Inoue, A. & Zhang, Y. Nucleosome assembly is required for nuclear pore
541 complex assembly in mouse zygotes. *Nat. Struct. Mol. Biol.* **21**, 609–616 (2014).
542 22. Ooga, M. *et al.* Changes in H3K79 methylation during preimplantation
543 development in mice. *Biol. Reprod.* **78**, (2008).
544 23. Egli, D., Birkhoff, G. & Eggan, K. Mediators of reprogramming: Transcription
545 factors and transitions through mitosis. *Nat. Rev. Mol. Cell Biol.* **9**, 505–516
546 (2008).
547 24. Kishigami, S., Van Thuan, N., Wakayama, S., Hikichi, T. & Wakayama, T. A
548 novel method for isolating spermatid nuclei from cytoplasm prior to ROSI in the
549 mouse. *Zygote* **12**, 321–327 (2004).
550 25. Bui, H. T. *et al.* Essential role of paternal chromatin in the regulation of
551 transcriptional activity during mouse preimplantation development. *Reproduction*
552 **141**, 67–77 (2011).
553 26. Abe, K. ichiro *et al.* Minor zygotic gene activation is essential for mouse

554 preimplantation development. *Proc. Natl. Acad. Sci. U. S. A.* **115**, E6780–E6788
555 (2018).
556 27. Quinn, P. & Begley, A. J. Effect of human seminal plasma and mouse accessory
557 gland extracts on mouse fertilization in vitro. *Aust. J. Biol. Sci.* **37**, 147–152
558 (1984).
559 28. Chatot, C. L., Lewis, L. J., Torres, I. & Ziomek, C. A. Development of 1-cell
560 embryos from different strains of mice in CZB medium. *Biol. Reprod.* **42**, 432–
561 440 (1990).
562 29. Wakayama, S., Kishigami, S. & Wakayama, T. Improvement of mouse cloning
563 from any type of cell by nuclear injection. *Methods Mol. Biol.* **1874**, 211–228
564 (2019).
565 30. Konno, S. *et al.* Removal of remodeling/reprogramming factors from oocytes and
566 the impact on the full-term development of cloned embryos. *Development* **147**,
567 (2020).
568 31. Lawitts, J. A. & Biggers, J. D. Culture of preimplantation embryos. *Methods*
569 *Enzymol.* **225**, 153–64 (1993).

32. Ooga, M. & Wakayama, T. FRAP analysis of chromatin looseness in mouse zygotes that allows full-Term development. *PLoS One* **12**, (2017).

33. Ooga, M., Funaya, S., Aoki, F. & Wakayama, T. Zygotic fluorescence recovery after photo-bleaching analysis for chromatin looseness that allows full-term development. *J. Vis. Exp.*, (2018).

578 **Supplemental materials**

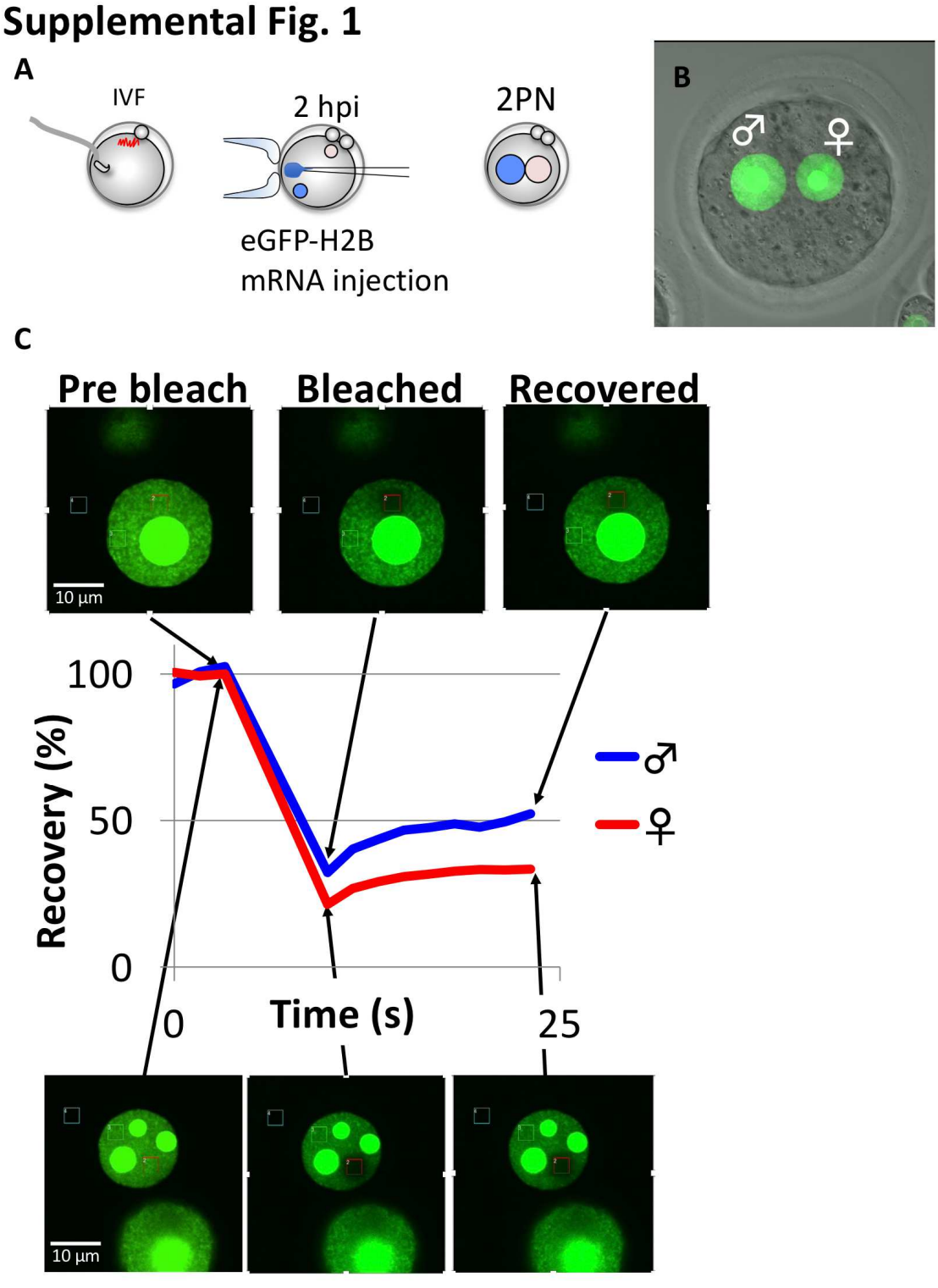

579

580 **Supplemental Fig. 1**

zFRAP analysis

(**A**) In our previous study, IVF-derived zygotes were microinjected with mRNA at 2 hpi. (**B**) At 8 hpi, parental PNs were easily distinguished by size, as a male PN is larger than a female PN. Sufficient expression of eGFP-H2B was confirmed. (**C**) For zFRAP analysis, a specific region of interest (ROI) in the PNs was selected and bleached. Red rectangle indicates bleached ROI, green is reference, and light blue is background. Compared to pre-bleaching, the fluorescence level drastically decreased after bleaching and then gradually recovered. Male PNs always exhibited greater fluorescence than the female PNs. Fluorescence levels at several points were plotted as a "recovery curve."

Supplemental Fig. 2

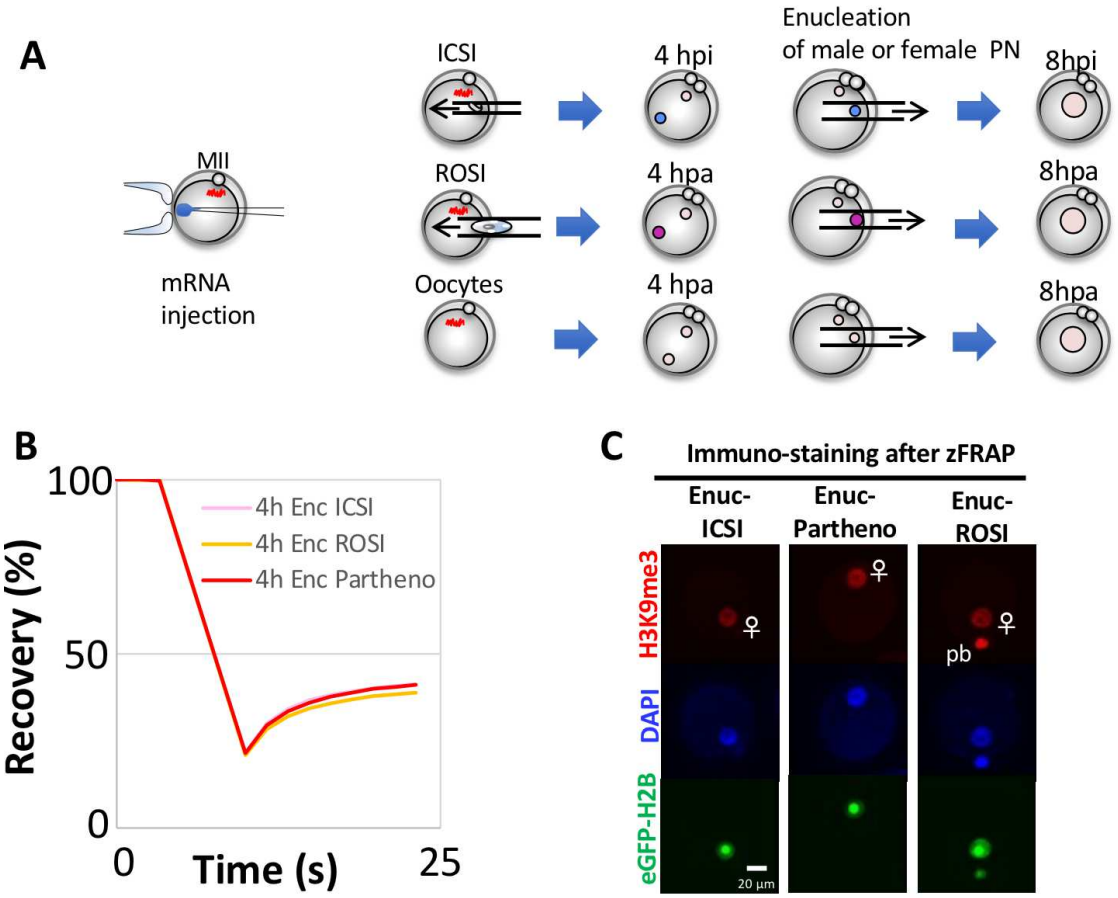

Supplemental Fig. 2

Dependency of chromatin compaction of fPN on sp-mPN

(**A**) Illustration of the preparation of mPN-enucleated partheno-zygotes at 4 hpi (**B**) Recovery curve of mPN-enucleated partheno-zygotes. (**C**) In order to confirm correct PN selection, after zFRAP analysis, the zygotes were subjected immuno-staining of H3K9me3, as a fPN marker.

Supplemental Fig. 3

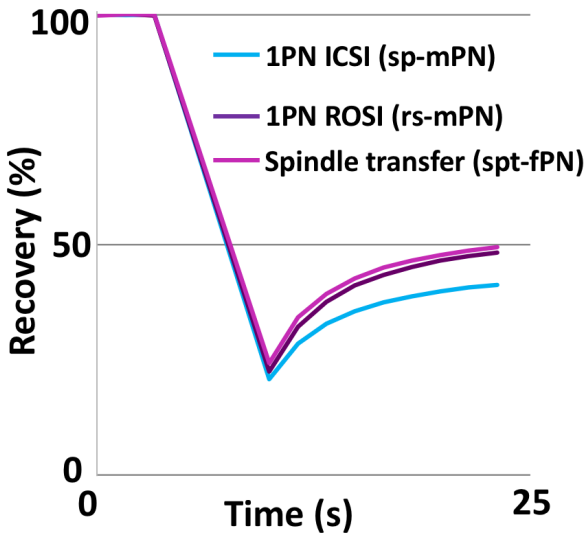

602

603 **Supplemental Fig. 3**

604 *Sperm-derived chromatin compaction ability functions to sp-mPN itself.*

605 Recovery curve of 1PN-zygotes. 1PN ICSI have only sp-mPN (sperm-derived mPN),

606 1PN ROSI have only rs-mPN (round spermatid-derived mPN), and spindle transfer have

607 only spt-fPN (spindle transfer-derived fPN).

608

609

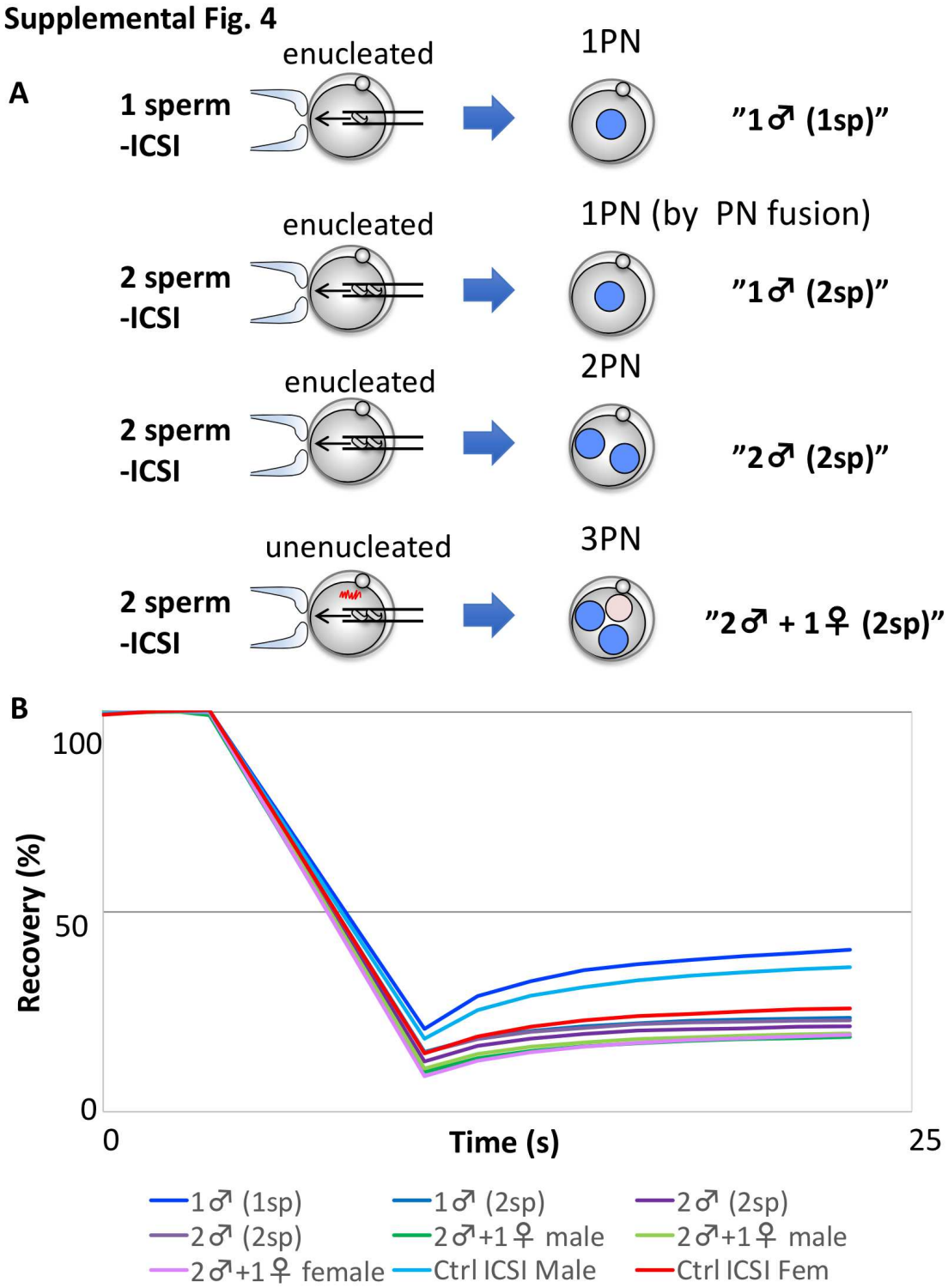

610

611 **Supplemental Fig. 4**

612 *Chromatin compaction is dependent on the number of microinjected sperm*

(**A**) Schematic illustration of the preparation of zygotes of "1♂ (1sp)," "1♂ (2sp)," "2♂ (2sp)" and "2♂ + 1♀ (2sp)." One or two sperm were microinjected into enucleated or un-enucleated MII oocytes. "1♂ (1sp)" indicates that one sperm was injected, which resulted in the formation of a single sp-mPN. (**B**) Recovery curves of ICSI-zygotes microinjected with one or two sperm.

Supplemental Fig. 5

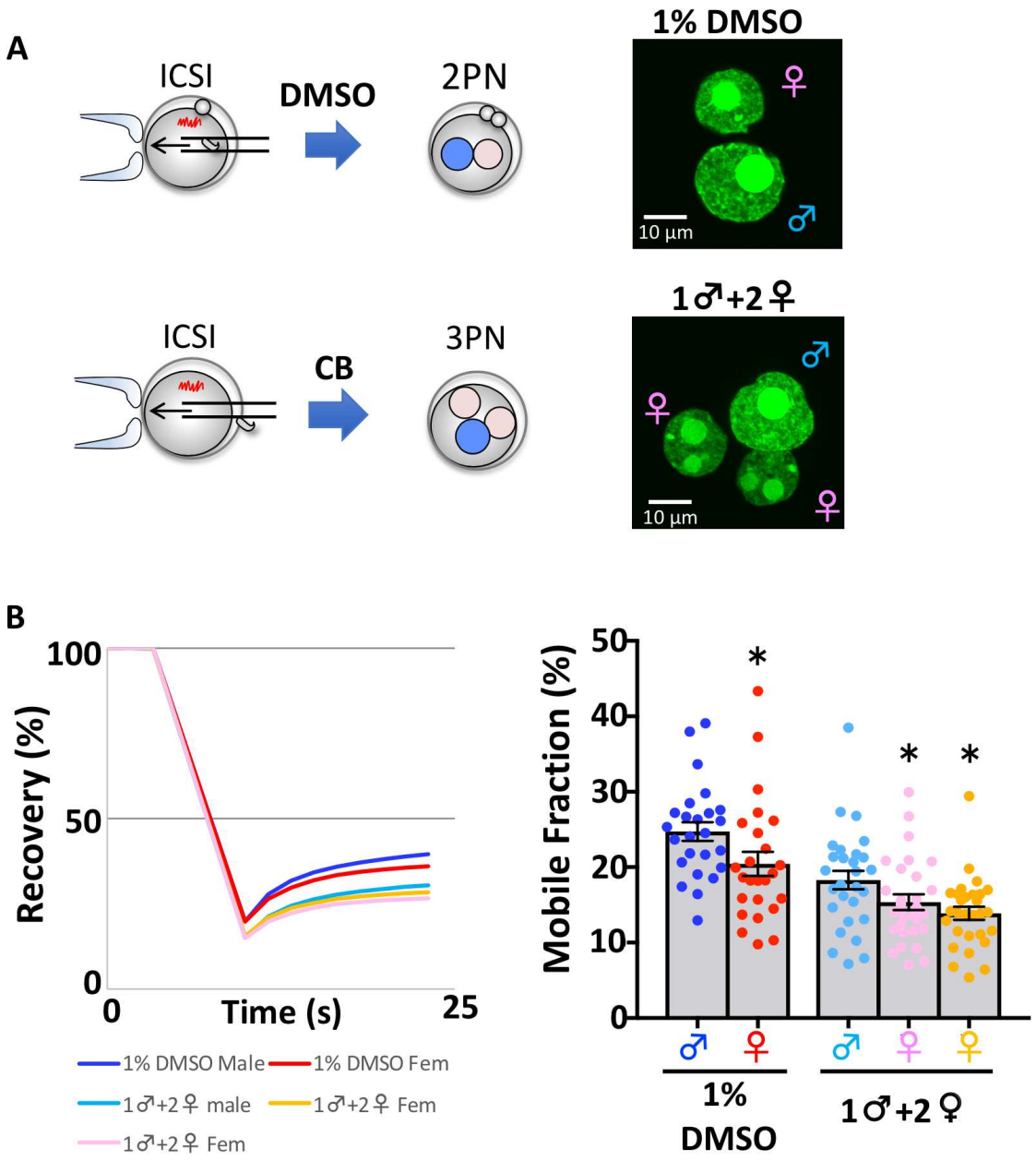

620

621 **Supplemental Fig. 5**

622 *Increases of fPN did not disrupt parental asymmetric pattern.*

623 (**A**) Schematic illustration of the preparation of zygotes of "1♂ + 2♀." CB is an inhibitor

624 of cytokinesis, which increases the fPN in the treated zygotes. Fluorescence images of

625 the zygotes are shown. Two fPNs are shown. (**B**) Recovery curve and average MF scores

626 of "1♂ + 2♀" and control zygotes are shown. Blue, red, light blue, pink, and orange dots
627 are MF scores of sp-mPN, fPN in control zygotes, and sp-mPN and two fPNs in CB
628 treated-zygotes, respectively.
629
630

Supplemental Fig. 6

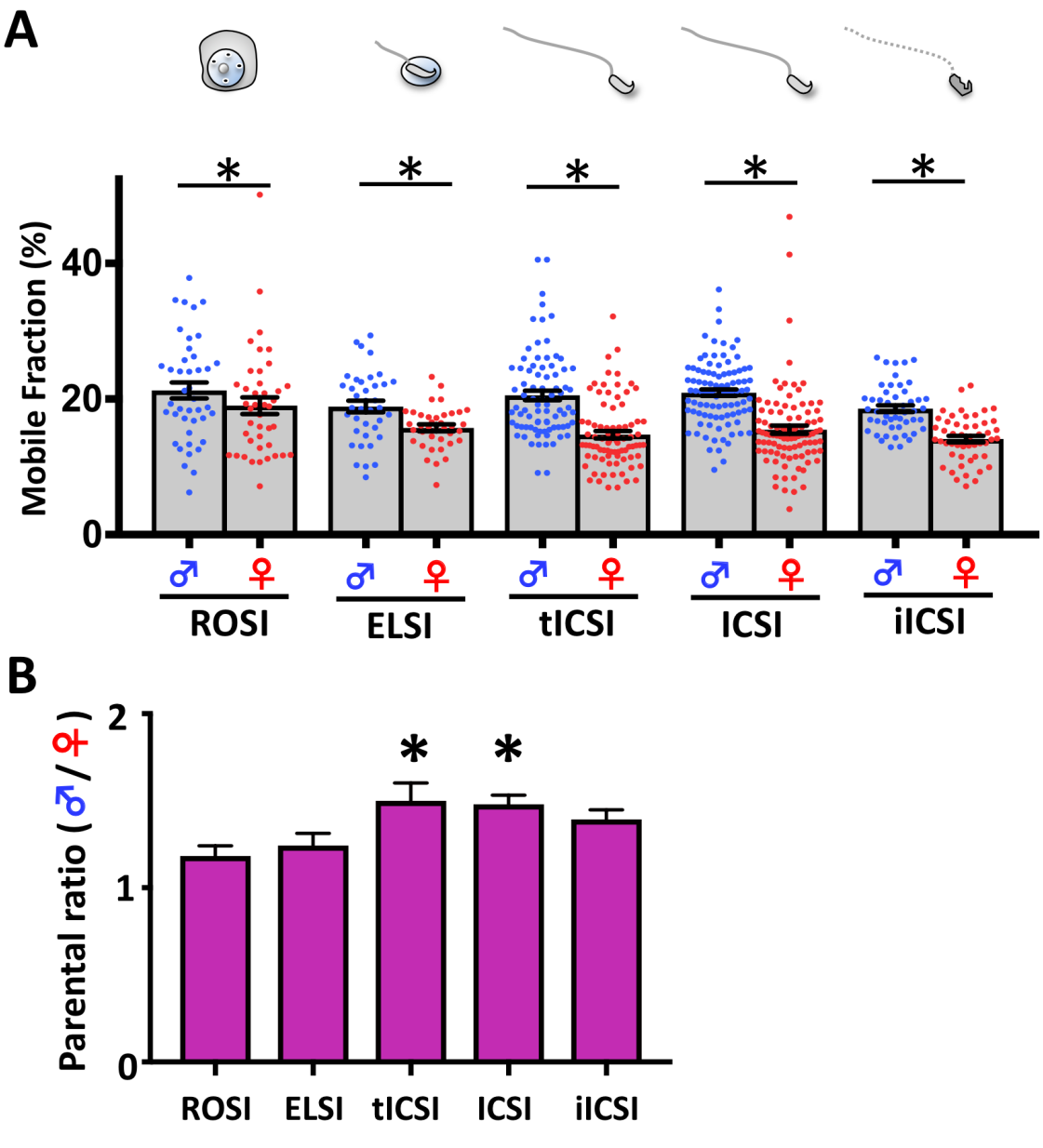

Supplemental Fig. 6

Male germ cells acquired the ability to compact chromatin and resistance during spermiogenesis

(**A**) zFRAP analysis with ROSI, ELSI, tICSI, ICSI, and ICSI with inactivated sperm (iICSI) was performed. The average MF scores of the zygotes are shown. Blue and red

637 dots are the MF scores of the mPN and fPN, respectively. (**B**) Bar graph of the average
638 MF score of the mPN/fPN ratio. The asterisks indicate significant differences as
639 compared with ROSI by one-way ANOVA followed by Tukey's multiple comparisons
640 test.
641
642

Supplemental Fig. 7

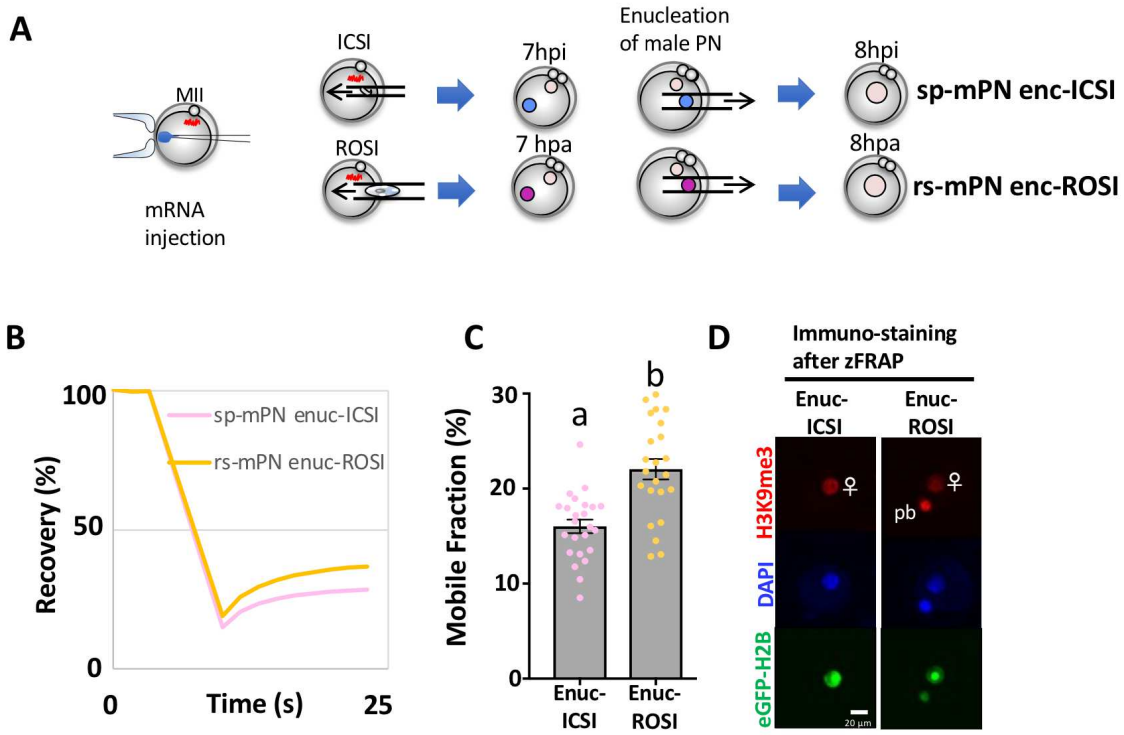

Supplemental Fig. 7

Round spermatid did not harbor chromatin compaction ability

(**A**) Schematic illustration of the preparation of ICSI- and ROSI-zygotes without mPN. (**B**) Recovery curve of mPN-enucleated ICSI-(sp-mPN enuc-ICSI) and ROSI(rs-mPN enuc-ROSI)-zygotes. (**C**) The average MF scores are shown. Pink and orange dots indicate the MF score of each fPN of the zygotes. (**D**) Immuno-staining of H3K9me3 in zygotes after zFRAP analysis. H3K9me3 signals indicating correct discrimination of parental PN during the enucleation process.

Supplemental Fig. 8

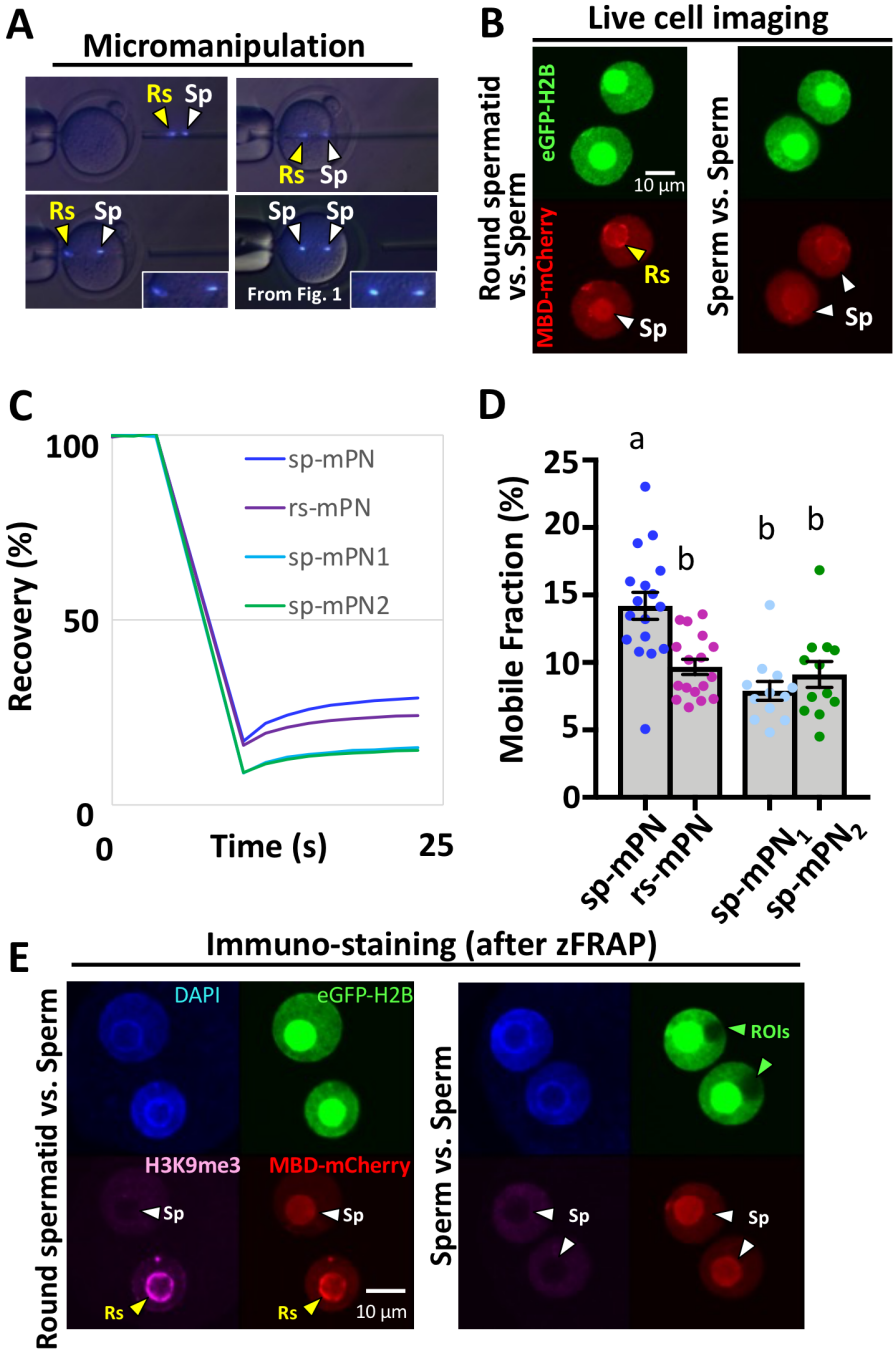

Supplemental Fig. 8

Round spermatids were not resistant to the chromatin compaction effect of sperm

(**A**) "Sperm head and round spermatid" or "sperm head and sperm head" were co-injected into the enucleated oocytes at the same time. Yellow "Rs" and white "Sp" indicate round

spermatid and sperm, respectively. The insets are images at higher magnification. DNA was stained with Hoechst. (**B**) MBD-mCherry expression in the live zygotes during zFRAP analysis. Upper panel is eGFP-H2B expression. Lower red panel indicates MBD-mCherry expression. Triangle indicates the perinucleolar ring where MBD-mCherry was enriched in male PNs derived from round spermatid but not sperm. (**C**) Recovery curve indicating the average fluorescence recovery rate. sp-mPN, rs-mPN, sp-mPN#1, and sp-mPN#2 indicate the score of male PN derived from round spermatid and spermatozoa, and co-injected spermatozoon, respectively. (**D**) MF scores of 2PN androgenic zygotes are shown. Gray bar graph of average MF values. Single dots indicate the mobile fraction score obtained from either mPN derived from round spermatid or sperm. Different characters indicate significant differences ($p < 0.05$, by one-way ANOVA and Tukey's multi comparisons test). Error bar indicates the SE.

(**E**) Immunocytochemial analysis with antibody against H3K9me3. To confirm discrimination of the derivation of male PNs using MBD-mCherry, since the marker for male PN derived from round spermatid, H3K9me3, was stained. Purple indicates immno-staining of H3K9me3, which only male PNs derived from round spermatid showed. Green triangle indicates the ROIs that were bleached during zFRAP analysis.

Supplemental Fig. 9

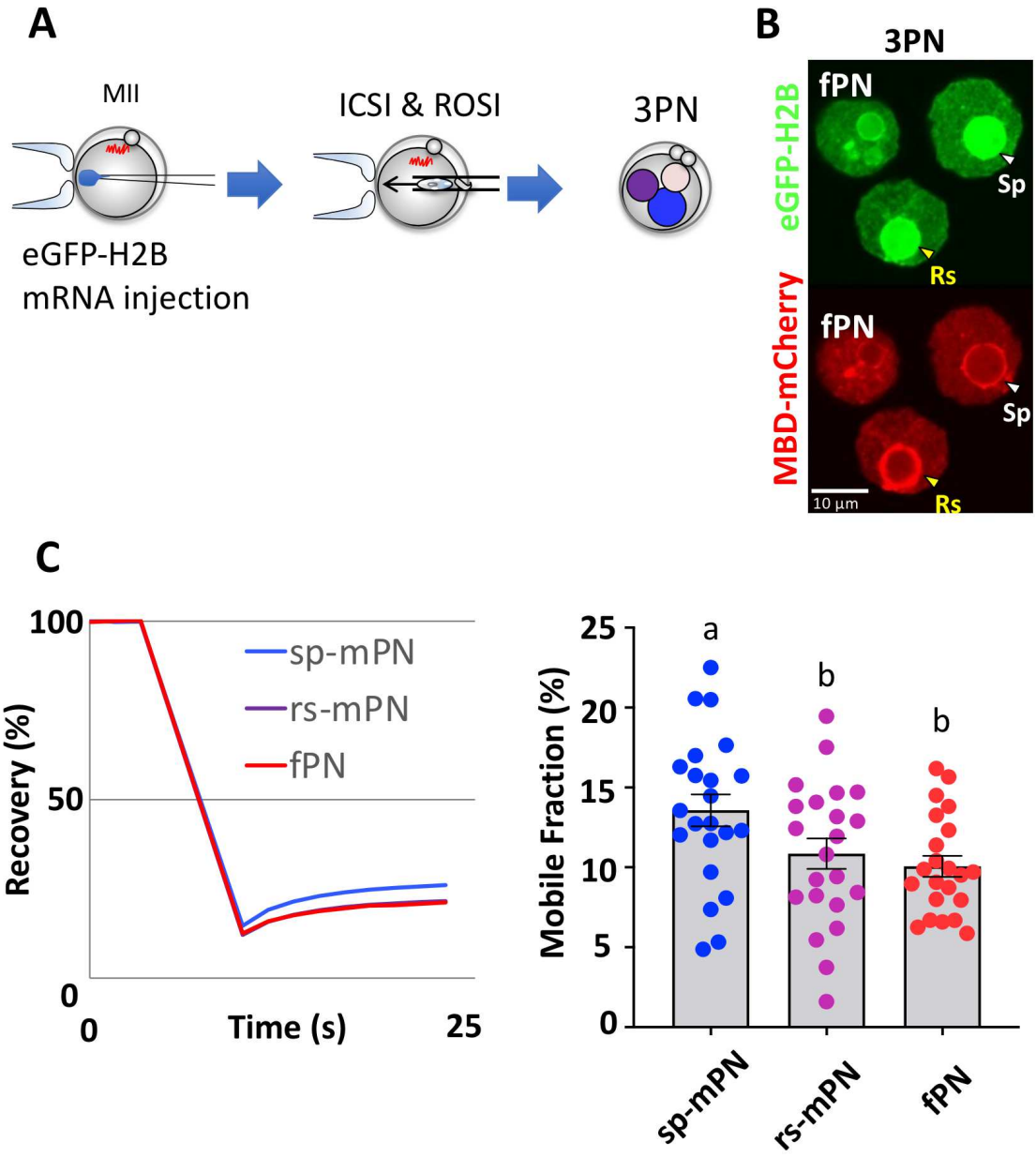

685

686 **Supplemental Fig. 9**

687 *Chromatin derived from round spermatid could be condensed to the same level as fPN*

688 (**A**) Schematic illustration of the preparation of zygotes with sp-mPN, rs-mPN, and fPN.

689 Sperm and round spermatids were co-injected into un-enucleated MII oocytes. (**B**)

690 Fluorescence image of zygotes harboring the 3PN. MBD-mCherry showed preferential

691 localization to the nucleolar ring of rs-mPN to distinguish the derivation of mPNs. (**C**),

692 (**D**) Recovery curve and MF scores of sp-mPN, rs-mPN, and fPN in 3PN-zygotes.

693

694

Supplemental Fig. 10

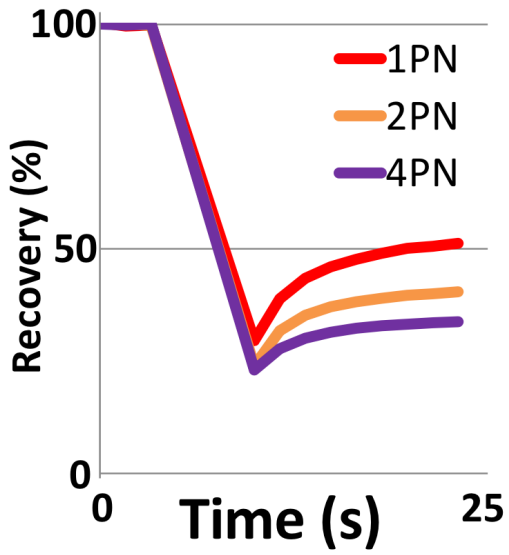

Supplemental Fig. 10

Recovery curve of 1, 2, and 4PN parthenogenetic zygotes.

Supplemental Fig. 11

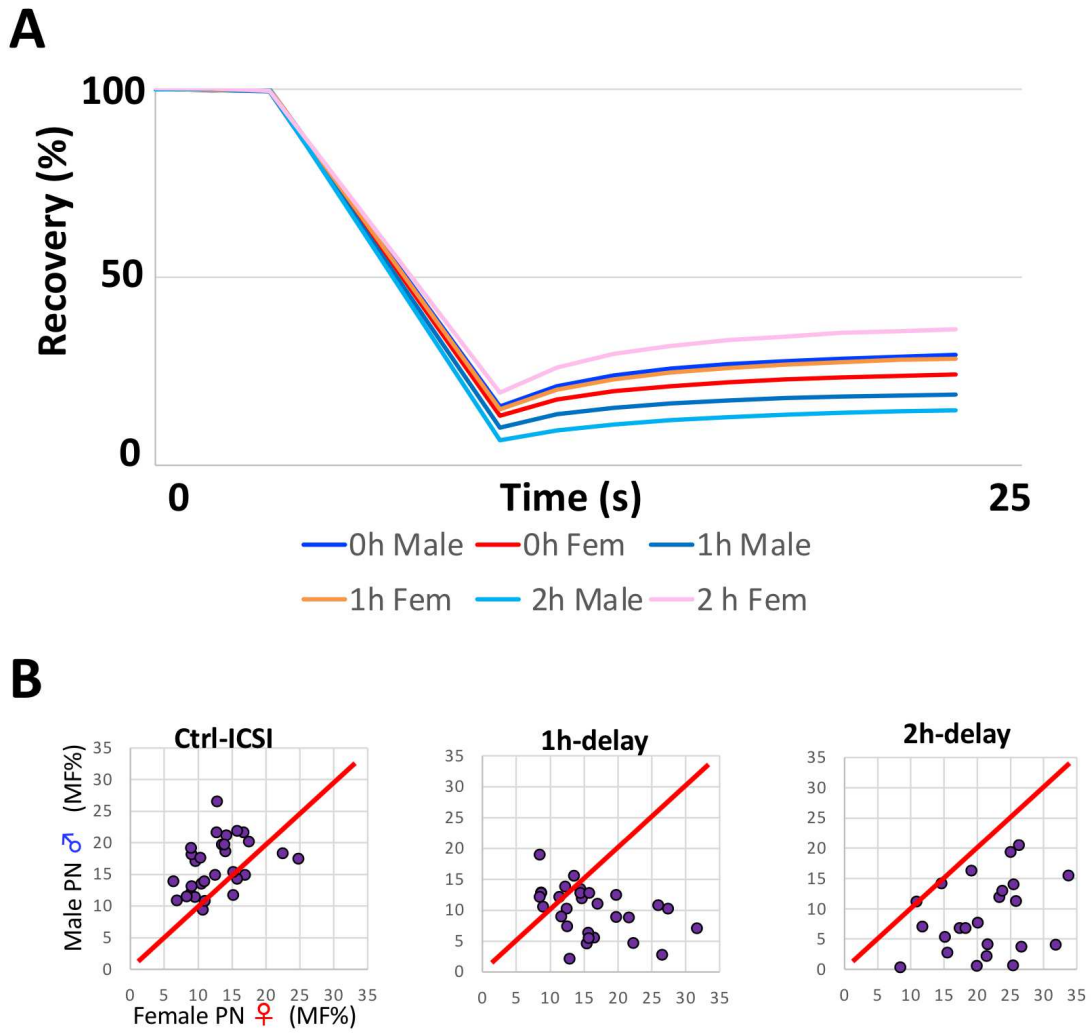

699

700 **Supplemental Fig. 11**

701 (**A**) Recovery curve of control and 1, 2 h-delay ICSI zygotes.

702 (**B**) Purple single dots indicate MF scores of parental individual pronuclei. Red line

703 indicates the ♂ = ♀ border line. Left side: ♂ > ♀, right side: ♂ < ♀.

704

705

706

707

Supplemental Fig. 12

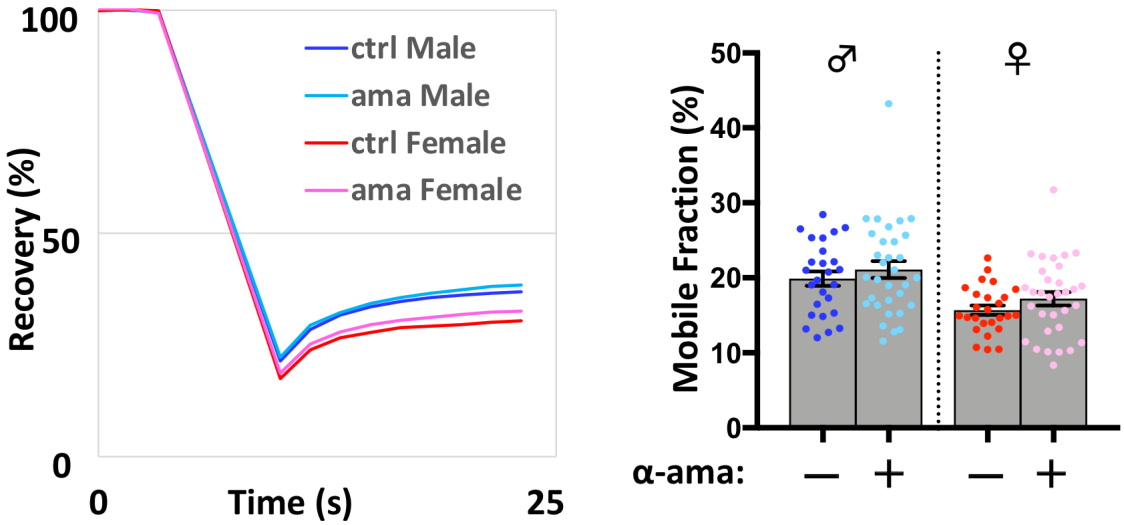

Supplemental Fig. 12

(**A**) Recovery curve of control and alpha-amanitin (RNA pol II inhibitor, α-ama) treated IVF-zygotes. Ctrl indicates non-treated zygotes. (**B**) The MF scores of the zygotes are shown in the bar graph.

Supplemental Fig. 13

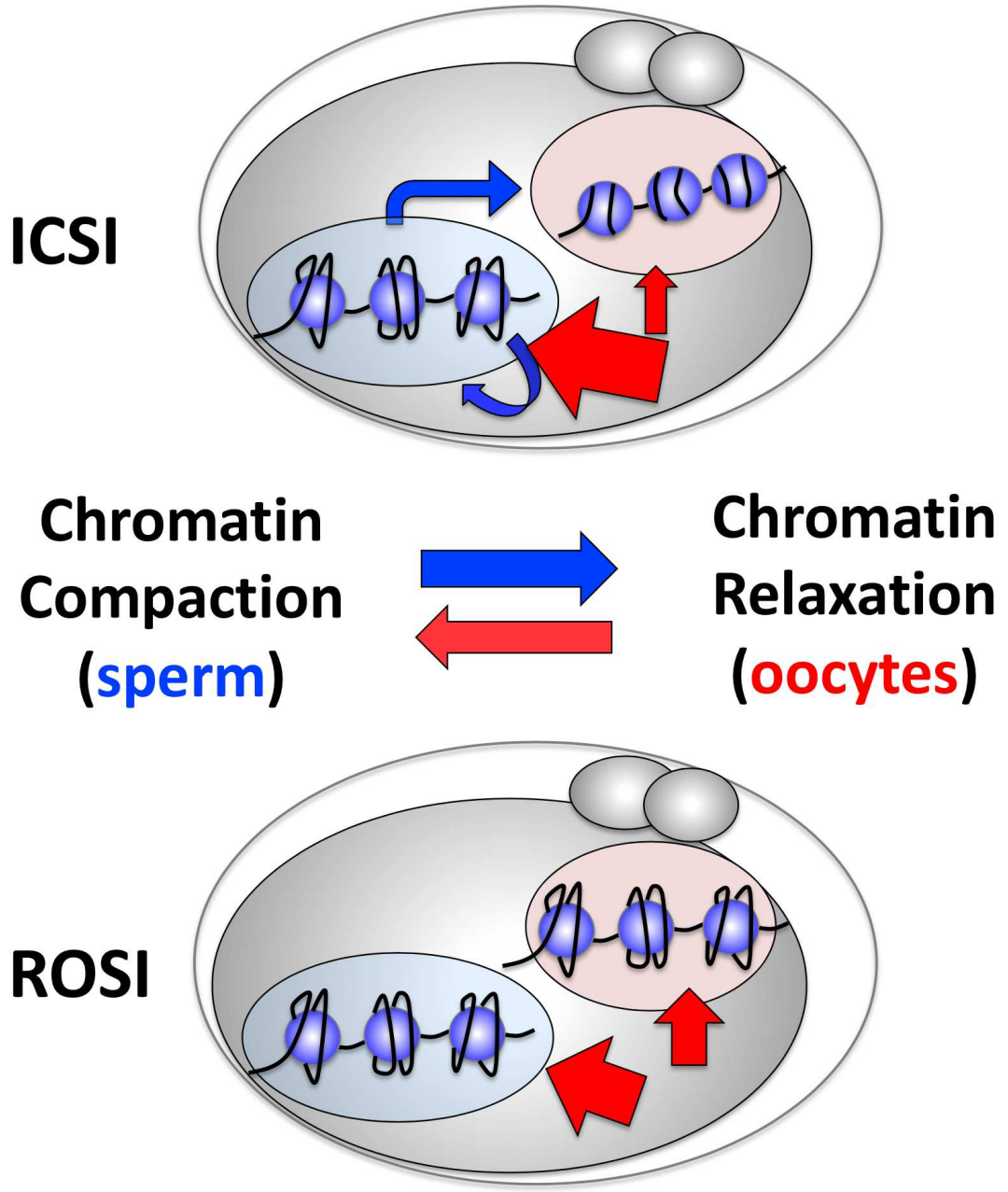

715

716 **Supplemental Fig. 13**

717 Schematic illustration of the hypothetical model in this study. In ROSI-zygotes, since
718 round spermatids lack the ability to compact chromatin, fPN could avoid chromatin
719 compaction. However, as described in the Discussion section, an rs-mPN may be able to

720 incorporate more maternal factors (including chromatin relaxer) from the cytoplasm,
721 resulting in a slightly more relaxed chromatin structure in an rs-mPN than a fPN.
722
723
724
725
726